Engineering Geology 341 (2024) 107735

Contents lists available at ScienceDirect

Engineering Geology

journal homepage: www.elsevier.com/locate/enggeo

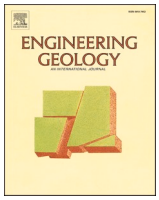

Sediment stacking pattern effect on sand liquefaction inferred from full-scale experiments in the Emilia alluvial plain (Italy)

Luca Minarelli [a,*], Daniela Fontana [b], Stefano Lugli [b], Kyle M. Rollins [c], Marco Stefani [d], Laura Tonni [e], Sara Amoroso [a,f]

[a] Istituto Nazionale di Geofisica e Vulcanologia, L'Aquila, Italy
[b] University of Modena and Reggio Emilia, Modena, Italy
[c] Brigham Young University, Provo, UT, USA
[d] University of Ferrara, Italy
[e] University of Bologna, Italy
[f] University of Chieti-Pescara, Pescara, Italy

ARTICLE INFO

Keywords:
Liquefaction
Stratigraphy
In situ tests
Blast tests
Sand composition

ABSTRACT

The geometry and the depositional configuration of sand bodies affected by the 2012 Emilia earthquakes (Bondeno site, northern Italy) were reconstructed and the role of the sediment stacking pattern was tested using data from full-scale blast experiments. The research integrates remote sensing and surface geological mapping, subsurface investigations including stratigraphic coring and cone penetration tests, grain-size and petrography of sands, geotechnical and geophysical monitoring. Data are compared with the Mirabello blast test site, also in the epicentral area. The results highlight the preeminent role of sediment heterogeneity and their mechanical and compositional properties in modulating liquefaction in alluvial settings. The lateral confinement of the buried sandy bodies, their thickness, and the occurrence of a thick non-liquefiable crust influence the dissipation of the excess pore water pressure, as indicated by the blast monitoring, and therefore the duration of liquefaction phenomena, according to the local stratigraphic architecture.

1. Introduction

During the last decades, several research studies were focused on the various geotechnical features controlling the potential for liquefaction (e.g. Ishihara, 1985; Idriss and Boulanger, 2008; Chang et al., 2011; Boulanger and Idriss, 2014; Hwanwoo et al., 2024; Bol et al., 2024), but few were related to the influence of the stratigraphic architecture on the liquefaction phenomena in different depositional environments. Most of these studies were developed in alluvial plains (e.g. Obermeier, 1998; Papathanassiou et al., 2015; Giona Bucci et al., 2018; Li et al., 2018; Fontana et al., 2019; Güven et al., 2023), others involved costal dunes as well as continental-marine, lacustrine and transitional sediments (e.g. Quigley et al., 2013; Salocchi et al., 2020; Kanibir et al., 2006). These studies reconstructed detailed stratigraphic models of the subsoil (Amorosi et al., 2016) providing information on the source layer that produced liquefaction surface features. However, these studies are mainly based on qualitative evaluation. We believe that to observe and understand how the depositional architecture may influence the mechanism of these coseismic effects, it is important to have direct measurements of the main physical parameters while the liquefaction is developing.

In this paper we combine core facies analysis and high-resolution stratigraphic correlations with in situ geotechnical data and controlled induced liquefaction experiment (blast test) in a research site near Bondeno (Ferrara, Italy). This has allowed us to reconstruct a detailed stratigraphic and geotechnical model, and for the first time to validate the model by comparing the liquefaction induced by natural events (2012 Emilia earthquakes) with full scale experiments (blast tests).

The observations derived from this study at Bondeno site were then compared with the blast test site at Mirabello (Ferrara, Italy), approximately 15 km south-eastward, where similar data were collected. The Mirabello site was also strongly affected by liquefaction, during the 2012 seismic sequence and then studied by monitoring the full-scale experimental test (e.g. Amoroso et al., 2017). The comparison between the Bondeno and Mirabello case studies has allowed us to observe the response of the measured parameters (e.g. pore water pressure, shear

* Corresponding author.
E-mail address: luca.minarelli@ingv.it (L. Minarelli).

https://doi.org/10.1016/j.enggeo.2024.107735
Received 4 June 2024; Received in revised form 21 August 2024; Accepted 22 September 2024
Available online 23 September 2024

wave velocity) in relation to the different depositional configurations, and to improve the understanding of the role of the sediment heterogeneity and mechanical properties in controlling liquefaction in an alluvial setting.

2. Geological framework

The liquefaction experiments in this study were carried out within Holocene fluvial sand bodies deposited on the Po river plain, the largest alluvial plain of Italy, corresponding to the foreland basin of the Southern Alps and the Apennine chain. The study area is located above the tectonic structures forming the buried external portion of the Apennines (Fig. 1). The structures consist of reverse and strike slip faults, ramp anticlines, and wider syncline folds, characterized by great structural complexity (Toscani et al., 2009), associated with the compressive deformation of the sedimentary sequences, during the Plio-Pleistocene. The Pleistocene and Holocene depositional units show large lateral variations of thickness and sedimentary facies, recording significant difference in subsidence rate, influenced by the ongoing tectonic deformation (Carminati and Martinelli, 2002; Stefani et al., 2018). The active faults generate significant seismic activity connected to shallow hypocentres (Michetti et al., 2012). In 2012 two mainshocks (Fig. 1) were triggered by two different faults, and were followed by several aftershocks (Pondrelli et al., 2012). The first and strongest seismic event took place on May 20th (M_w 6.1, Finale Emilia) and the second on May 29th (M_w 5.9, Mirandola). The seismic waves generated widespread liquefaction and lateral spreading (Fig. 1). Coseismic liquefaction mainly developed within sand and silty sand bodies in the subsurface, within the first 15 m, associated with fluvial paleochannels and crevasse splays (Civico et al., 2015; Minarelli et al., 2022). The fluvial bodies may have a ridge-like, slightly elevated geomorphological expression, or may outcrop at the plain level.

The study area is located at the confluence between the Po River and several Apennine rivers, namely Secchia, Panaro and Reno (Fig. 1).

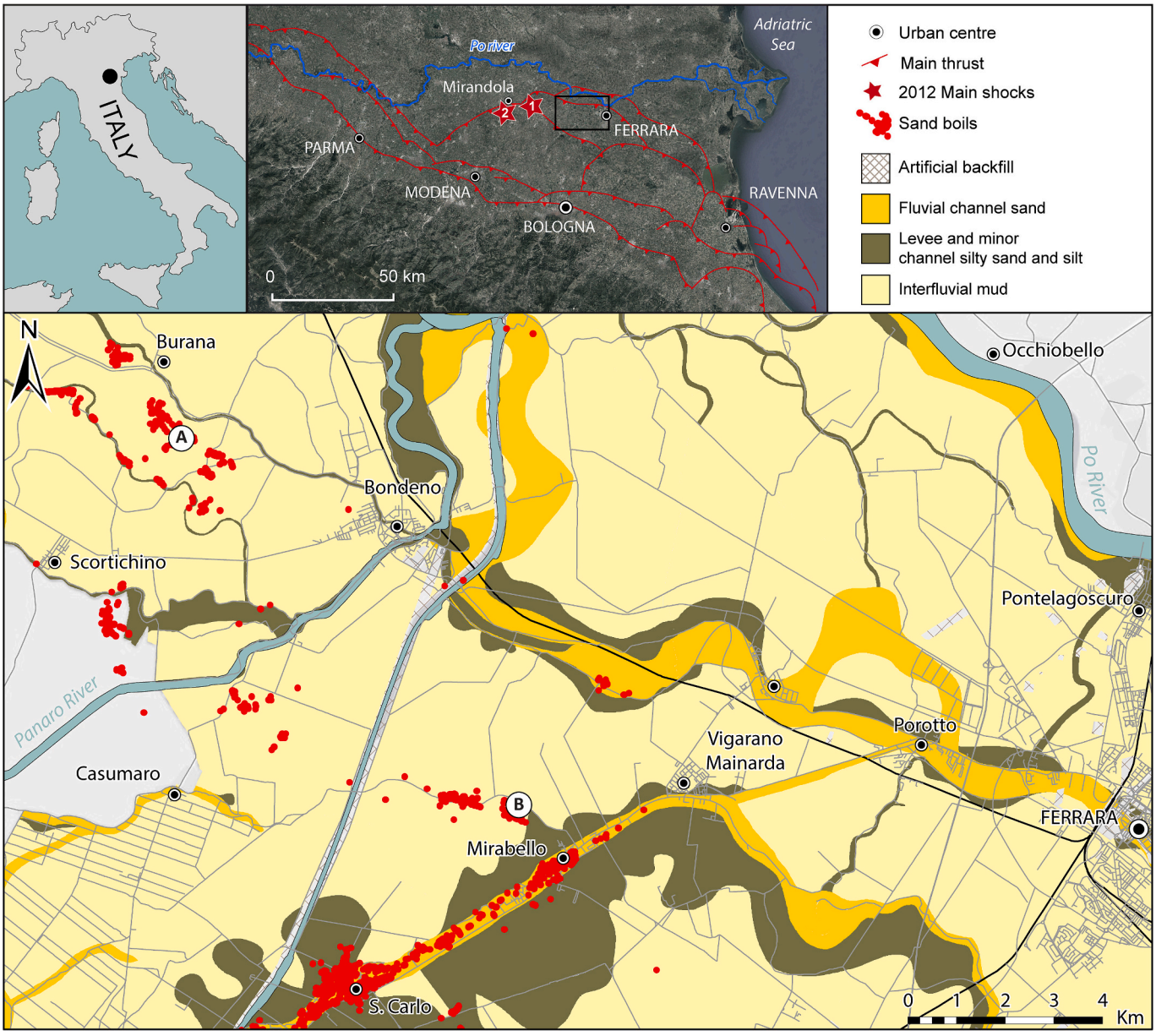

Fig. 1. Geological map and location of the study area illustrating the 2012 liquefaction phenomena (modified after Di Buccio et al., 2023). The case study of Bondeno, object of this study, is indicated by "A", and it is compared with the test site of Mirabello "B". Liquefaction data points are from EMERGEO Working Group (2013).

During the Holocene, the Po River formed a meander belt, with well-developed point-bar units, often reworking the underlying late Pleistocene synglacial coarse sands, accumulated in braided river settings. The last millennia saw an upstream shift of the Po meander belt and the development of channels elevated above the plain. The Apennine rivers form raised fluvial ridges, interspaced with wider interfluvial depressions. The late Pleistocene synglacial deposits are framed in the upper portion of the allostratigraphic unit named Villa Verucchio Subsynthem (AES7), overlain by a sharp pedogenized surface, recording a buried terraced morphology (Stefani et al., 2018). The Holocene alluvial plain sediments are included in the Ravenna Subsynthem (AES8).

3. Data sources and methods

3.1. Geological surface mapping and subsurface investigations

Geomorphology of the sedimentary bodies was investigated by radar altimetric data at regional scale and by a high-resolution digital model derived from an airborne LIDAR survey (Fig. 2a). The distribution of the surface sediments was inferred by examining a diachronous series of satellite and aerial images, acquired in the visible and near infrared spectrum, associated with field geological surveys and surface soil sampling. (Fig. 2b).

The dating of outcropping fluvial channel bodies accumulated through the last millennia is provided by archaeological data and written historiographic sources. Radiocarbon dating performed on an organic rich layer constrained the stratigraphic chronology in the Bondeno site.

The reconstruction of the stratigraphic architecture of the area surrounding the Bondeno test site was also possible thanks to the availability of (1) mechanical cone penetration tests (CPT), piezocone tests (CPTU), and seismic piezocone tests (SCPTU) from the seismic microzonation of the municipality (CPTUC, CPTUD, CPTUG, see Fig. 2); (2) the boreholes and CPTU tests carried out for the blast test experiment between December 2017 and January 2018 (S01, S11, CPTU500, CPTU501, CPTU502, CPTU01, CPTU11, see Figs. 2 and 3, further details in Amoroso et al., 2020, 2022). Moreover, boreholes and CPTUs were also performed for the present study in June 2018 (S500, S501, CPTU503, CPTU504, see Fig. 2) to extend the subsoil characterization of the study area.

3.2. Blast test measurements

The blast test experiment consisted of a sequence of controlled detonations to induce liquefaction in the natural deposits of the Bondeno area, previously liquefied in the 2012 earthquake, and to verify the effectiveness of a ground improvement technique in an adjacent subsoil treated with rammed aggregate piers (Amoroso et al., 2020, 2022, 2024; Rollins et al., 2021; Pesci et al., 2022). These two zones, the natural panel and the improved panel, were thoroughly characterized before the pier installation and before the blast tests (S11 and CPTU11 for the natural panel, CPTU01 and S01 for the improved panel, see Fig. 3). A total of 16 explosive charges, eight of 0.5 kg at 3.5 m and eight of 2.0-kg charges at 6.5 m in depth within the estimated potentially liquefiable layer, were detonated sequentially at 1-s intervals around the periphery of two 10-m-diameter circles at each test panel. Fig. 3 shows the blast hole soundings through which sand ejecta traveled after blasting (BH11, BH12, BH14, BH18, BH02, BH03). The monitoring of the blast-induced liquefaction was also carried out by the installation, inside the blast circles, of (1) a seismic dilatometer located at 6.1 m depth for shear wave velocity (V_S) measurements (SDMT blast, see Fig. 3), and (2) pore pressure transducers at depths between 4 and 9 m for the data acquisition of the excess pore pressure ratio ($R_u = \Delta u/\sigma'_{v0}$, where Δu is the measured excess pore water pressure and σ'_{v0} is the initial vertical effective stress prior to the blasts). Sand was also ejected during and after blasting through the holes of some pore pressure transducers, namely PPT4, PPT5 and PPT8 (Fig. 3).

3.3. Sampling

Three core holes S01, S11 and S501 (locations shown in Fig. 2), extending to depths of 15, 6 and 5 m, respectively, have been analyzed and sampled for the characterization of the depositional elements and geotechnical parameters. Each core hole has been described in terms of

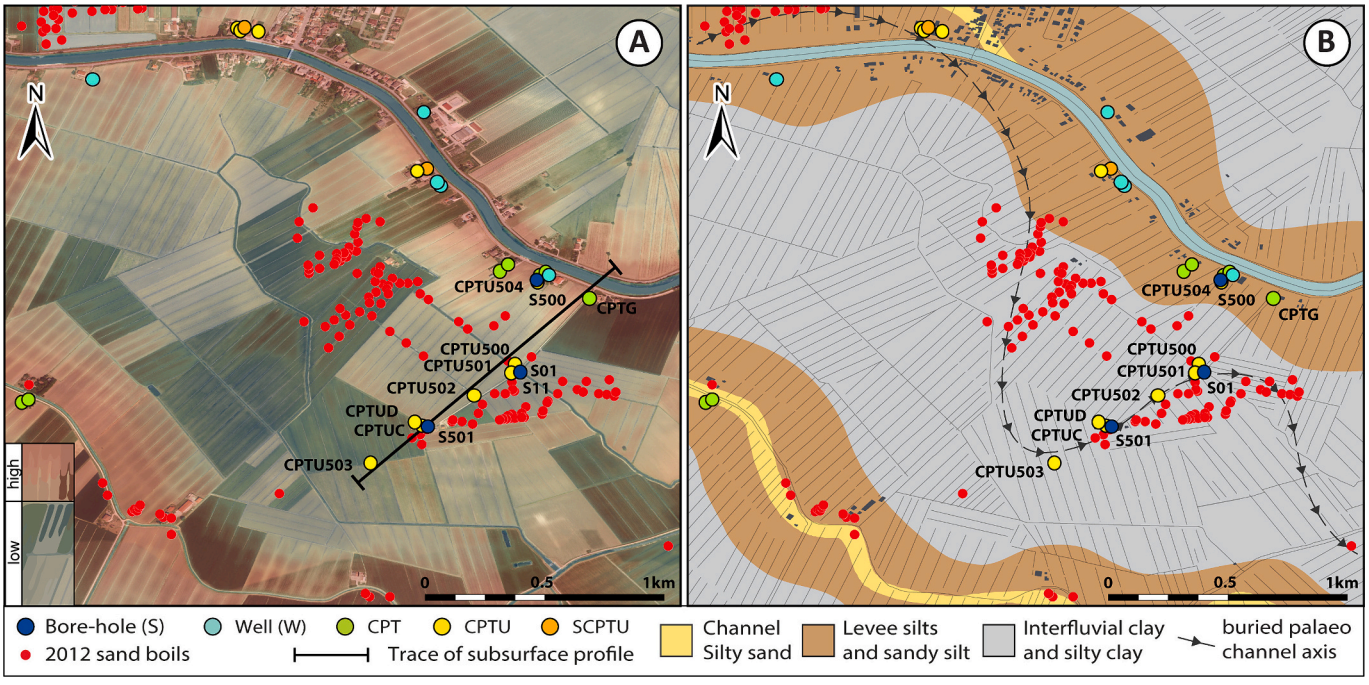

Fig. 2. Bondeno test site location with in situ geotechnical tests and the 2012 sand boils: (a) geomorphological features from combined LIDAR and satellite image, (b) surface lithological map of alluvial deposits.

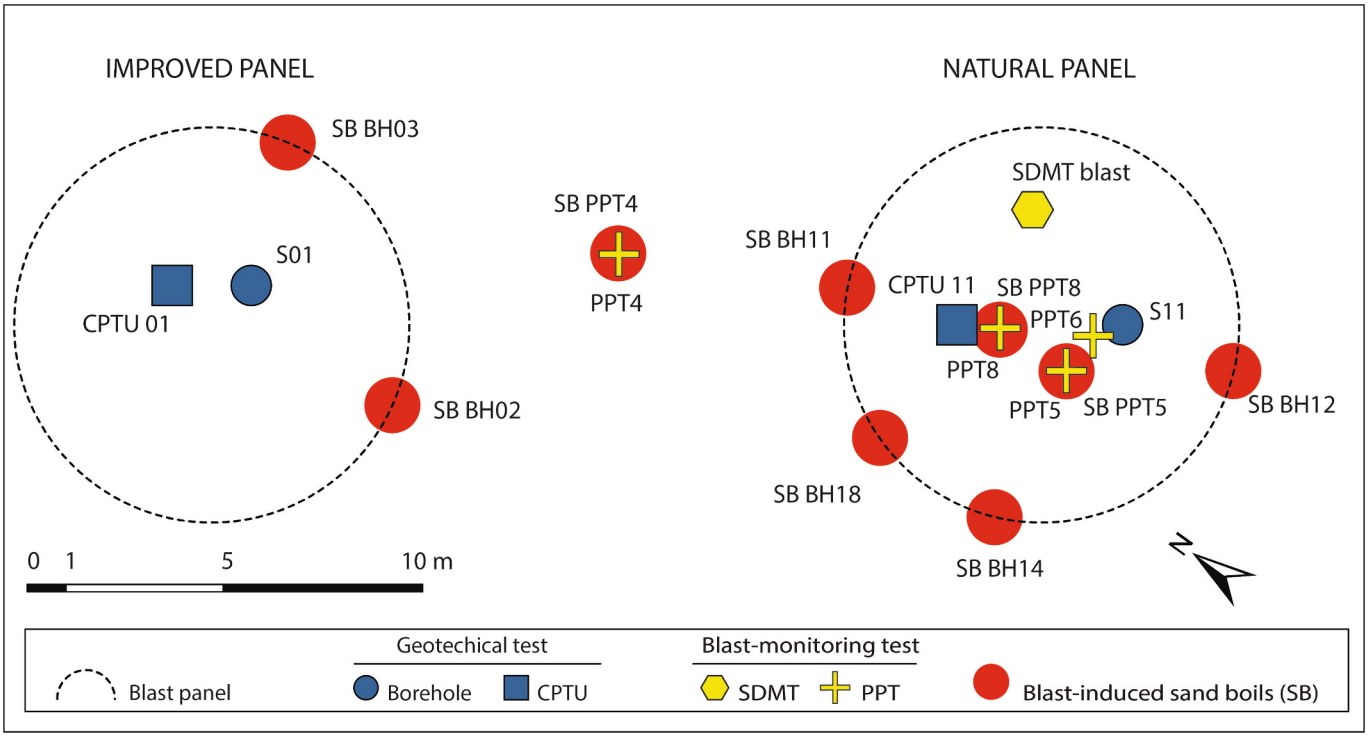

Fig. 3. Plan view of the blast test natural and improved panels with location of (1) boreholes and CPTUs performed before treatment and blasting, (2) seismic dilatometer (SDMT) acquiring during and after blasting, and (3) blast holes (BH) and pore pressure transducers (PPT) through which sand was ejected to the ground surface during and after blasting.

lithology, grain-size, color, and consistency. A total of 18 sand samples were selected from the cores (percent of core recovery in coarse-grained sediments >75 %) for analysis, at intervals of about one sample per meter.

Sand boils were sampled (nine samples) considering lateral and vertical grain-size variation. The samples from the largest boils have been divided into three sub-samples from the lower, middle, and top portions of the volcano structures (i.e. SBPPT5L, SBPPT5M, SBPPT5U, and SBBH11B, SBBH11A). Single samples are representative of the entire vertical sequence of the volcano flank close to the vent. The sedimentological and stratigraphic interpretation of the test site benefits from the comparison with the nearby S500 core.

3.4. Grain-size analyses

A total of 27 samples were analyzed using standard techniques: mechanical sieving for the sandy fraction and hydrometer analysis for fine-grained sediments. Sand samples, consisting of a few hundred grams, were washed with dilute H_2O_2 to remove organic matter, and then air dried and mechanically sieved for granulometric and compositional analyses.

Grain-size analyses are reported as granulometric curves, and index parameters are calculated in terms of: the fines content (FC) is the percentage of particles finer than 0.075 mm; D_{60}, D_{30}, and D_{10} sizes are the diameters of the 60th, 30th, and 10th percentiles of the granulometric curve; the coefficient of uniformity U is given by the ratio of D_{60} to D_{10}, and the coefficient of curvature C is a function of D_{30}, D_{60}, and D_{10}. According to the Unified Soil Classification System (USCS classification, ASTM D-2487-11, 2011, ASTM D2488–09, 2009) the sands characterized by $U > 6$ and $1 < C < 3$ are well graded (or poorly sorted).

3.5. Compositional analyses

Petrographic analyses were carried out on 23 sand samples: eleven samples were collected from core S01, two from core S11, and three from core S501. Six samples are from sand boils to document the source layer and compositional variations. The modal analyses of cores were compared with detrital modes of samples collected from modern rivers of the area: Po, Secchia, Panaro and Reno rivers (Lugli et al., 2004; Bruno et al., 2021; Demurtas et al., 2022), and with data from the Mirabello test site (Fontana et al., 2019). The sand fraction 0.250–0.125 mm was impregnated in epoxy resin under vacuum and processed to obtain thin sections. Point counting of 300 grains for each thin section was performed under transmitted-light microscopy according to the Gazzi-Dickinson method, designed to minimize the dependence of the analysis on the grain-size. Although all grain components were analyzed, only those with similar hydraulic behavior (quartz, feldspars, and lithic fragments: volcanic, metamorphic, and sedimentary) were considered for provenance analyses. The results of the modal analysis were plotted in the Q + F (quartz and feldspar) – L (siliciclastic lithic) – C (carbonate lithic) ternary diagram.

4. Results

4.1. Stratigraphic cores and cone penetration tests

The geological interpretation of the Bondeno blast test site was based on the stratigraphic correlation using continuous coring and CPTU soundings (Fig. 4).

In core S01, from top to bottom, several units were identified:

- an interval reworked by ploughing (0–0.45 m);
- an argillaceous layer with silt intercalations, plant remains and bioturbation, recording a moist interfluvial depression (0.45–3 m);
- a silt and sandy silt interval with subordinate clay levels and diffuse pedogenesis alteration, recording a drained interfluvial area (3–3.5 m);

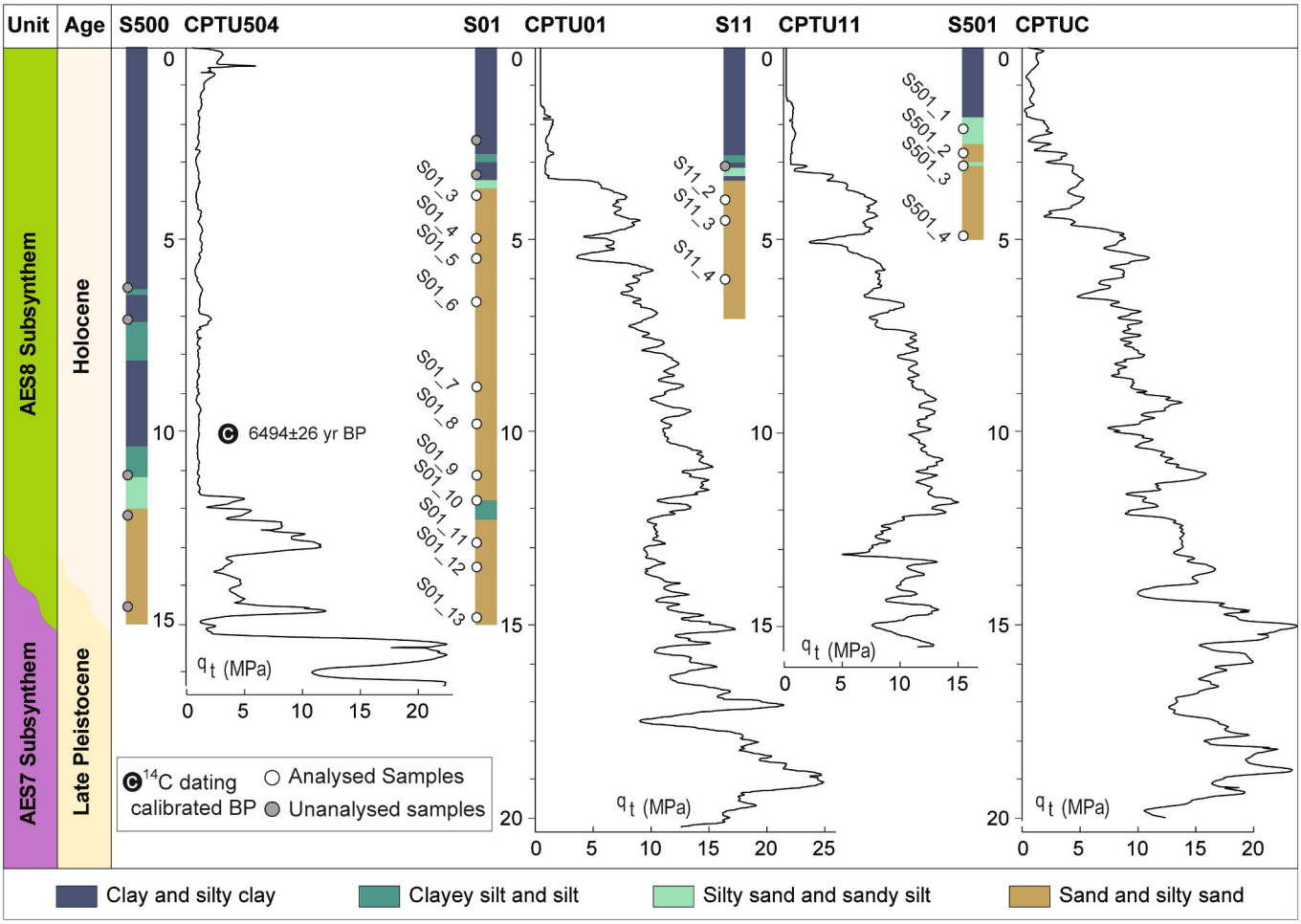

Fig. 4. Integrated stratigraphy from cores and CPTU logs at the Bondeno study area. A detailed description of the lithological intervals and depositional facies interpretation is provided in the text.

- the middle part of the cores (3.5–11.5 m) is referable to a fluvial meander and consists of fine and medium-coarse sand, with silty sand and silt intercalations in its upper portion, with sparse wood fragments; tractive laminations are locally preserved;
- 50 cm-thick silty interval (11.5–12 m);
- the lower part of the core records synglacial middle alluvial plain braided river environments and consists of coarse to medium grained sand (12–14.5 m) and fine silty sand (14.5–15 m).

The same stratigraphy was observed in the nearby core S11.

Two additional cores (S500 and S501, Fig. 4) were analyzed to better reconstruct the stratigraphic architecture of the area, at 500 m northward and 500 m southward of the test site. The core 501 (Fig. 5) is 5 m deep and it shows coseismic liquefaction probably associated with the 2012 seismic event. From the top:

- topsoil reworked by ploughing (0–0.45 m);
- brown silty clays with reddish patches, induced by water level fluctuations, pedogenetic carbonate concretions, organic and peat lenses (0.45–1.9 m);
- gray sandy silts and silty fine sands with brick fragments (1.9–2.5 m); gray sandy silts and silty fine sands with dikes of medium-coarse liquefied sands, indicating the path of the ejecta from beds preserved at the bottom of the profile, brick fragments are present at 1.9 m and at 2.3–2.5 m (Fig. 5a), possibly referable to Roman times settlement;
- gray medium-coarse sands with organic and silty lenses and liquefaction evidence consisting of flames and fractures filled by ejected sands (2.5–2.95 m, Fig. 5b);
- gray sandy silts and silty fine sands with injections of medium-coarse liquefied sands (2.95–3.4 m);
- gray medium-coarse sands with organic lenses (3.40–5 m).

Significant lateral variations in the stratigraphic succession were observed in the core S500, located 500 m north of the blast area. The core, 15 m deep, is characterized by:

- a 10 m-thick argillaceous unit of interfluvial depression, with three layers containing pre-Medieval ceramic fragments. At 10 m depth, 14C dating provides a calibrated age of 6494 years B.P.;
- a 2-m thick layer of gray sandy silt and silty sand;
- the deepest portion is made up of 3 m of gray medium-coarse sands, probably from synglacial environment.

The results of the CPTU data are in agreement with the stratigraphic logs, as recently discussed also by Li et al. (2018) for layered soils. For graphic simplicity, only the cone tip resistance values (q_t) are here depicted (Fig. 4), but the whole of the penetration data was analyzed in interpreting the profile. The boundary between the late Pleistocene and the Holocene has been supposed on the base of the available site investigations (mainly CPTU profiles) and dating.

Based on the in situ geotechnical investigations at the Bondeno site (Amoroso et al., 2022), the ground water table (GWT) shows minimal

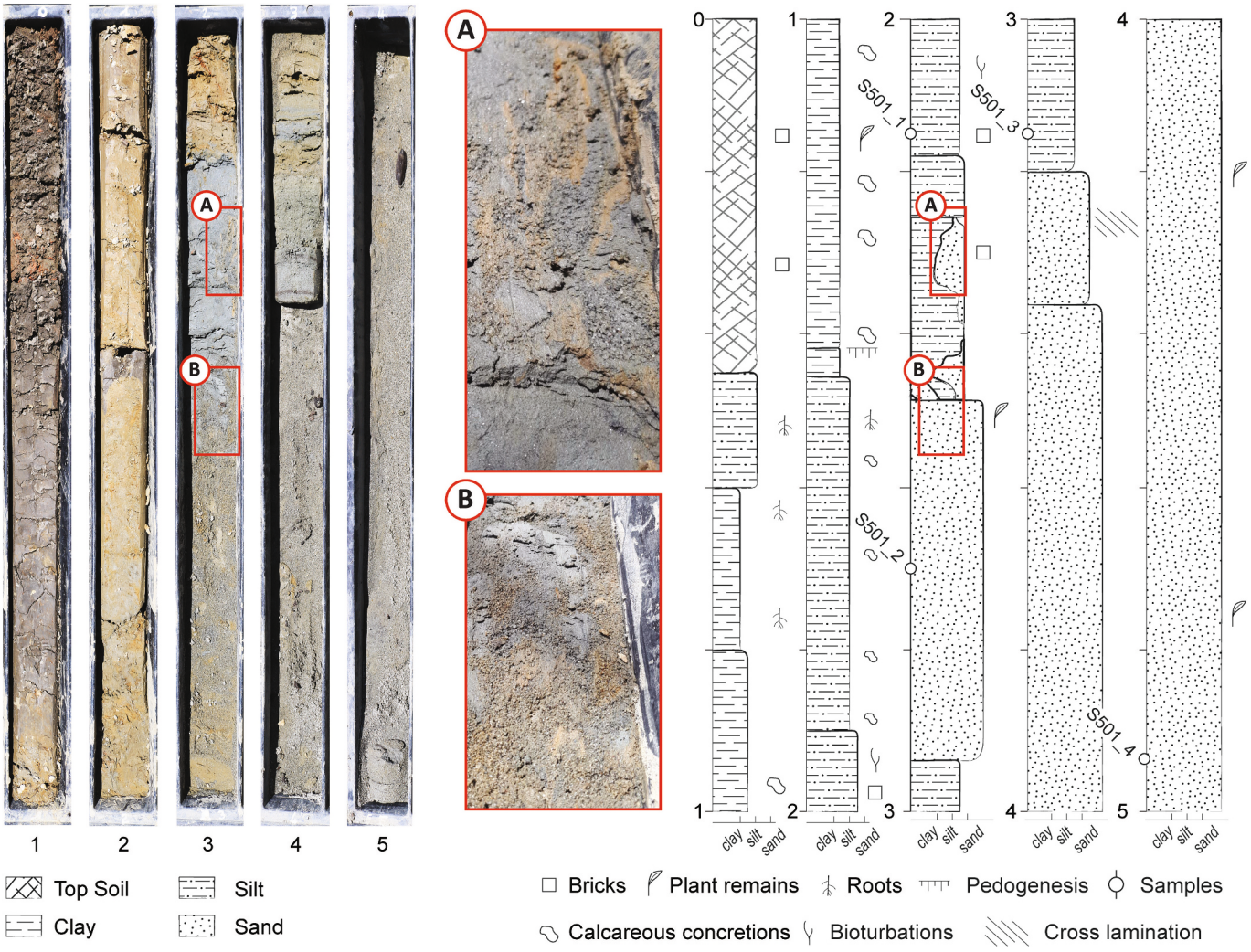

Fig. 5. Core picture and stratigraphic log of the S501 core and close-up view (A, B) of the interval with evidence of liquefaction (sand-filled fractures and flames).

seasonal variations ranging from 0.5 to 1.5 m below the ground level. Similar small variations are typical of this sector of the Po plain including Mirabello (e.g. Amoroso et al., 2017).

Geotechnical investigations were also used to obtain continuous profiles of the hydraulic conductivity k, by adopting a well-established CPTU-based empirical approach proposed by Robertson (2010). As known, the method allows calculating k as a function of the soil behavior type index I_{cn}, which in turn depends on the dimensionless, stress-normalized cone resistance Q_{tn} and friction ratio F_r. Recent site investigation campaigns carried out in testing areas located nearby (e.g. Bertolini et al., 2022; Tonni et al., 2024) have proved the reliability of the method in the determination of permeability characteristics of the Po river basin subsoil, hence the application of the correlations to the Bondeno sediments.

As a representative example, the profile obtained from interpretation of CPTU01, adjacent to borehole S01, is provided in Fig. 6a. In the fine and medium-coarse sand from 3.5 to 11.5 m in depth, the predicted permeability was found to vary in a rather narrow range between 10^{-5} and 10^{-4} m/s, with a mean value of $\log_{10}(k)$ equal to −4.24 (corresponding to $5.75{\cdot}10^{-5}$ m/s) and standard deviation $\sigma_{log10(k)}$ equal to 0.18. Thin intercalations of silty sands and silts, detected in the upper portion of this soil unit, are instead characterized by values of permeability in the range $1.74{\cdot}10^{-6}$–10^{-5} m/s. Below 12 m, estimates of k still fall in the range 10^{-5}–10^{-4} m/s, though being on average slightly lower than the values computed in the upper sandy unit. The higher scatter observed in predictions below 14 m is likely to be attributed to a more significant content of fine sands and silty fraction.

For useful comparison, CPTU-based estimates of the permeability obtained for the Mirabello test site are also shown in Fig. 6b. It is worth mentioning here the significant scatter of the computed values in the soil layer between 4 and 8 m in depth, whereas an approximately constant trend can be observed below 8 m. Further details will be provided later on in this paper.

4.2. Sand boil structures

Following the blast experiment, nine sand blows formed, six within the natural panel, two near the edge of the improved panel, and one in between the panels (Fig. 3). Two well-developed sand volcanoes in the middle of the natural panel are flat cones roughly circular-shaped, with a maximum width of about 2 m, and a maximum height of 10 cm (Fig. 7). They consist mostly of medium- to coarse-grained sand levels with a multiple direct-inverse gradation. Fig. 7b shows the transition from coarse grains in the basal portion passing to finer and again coarser in the upper portion. A thin fine-grained veneer, a few mm-thick, may also occur on top (Fig. 7c). This structure differs from the sand boils described for the 2012 Emilia earthquake, which consisted of various laminated sand layers: at least six sand/mud couplets were visible, indicating repeated fluctuations in the sediment/water flux, possibly due to multiple opening and closing of the fracture (Fontana et al.,

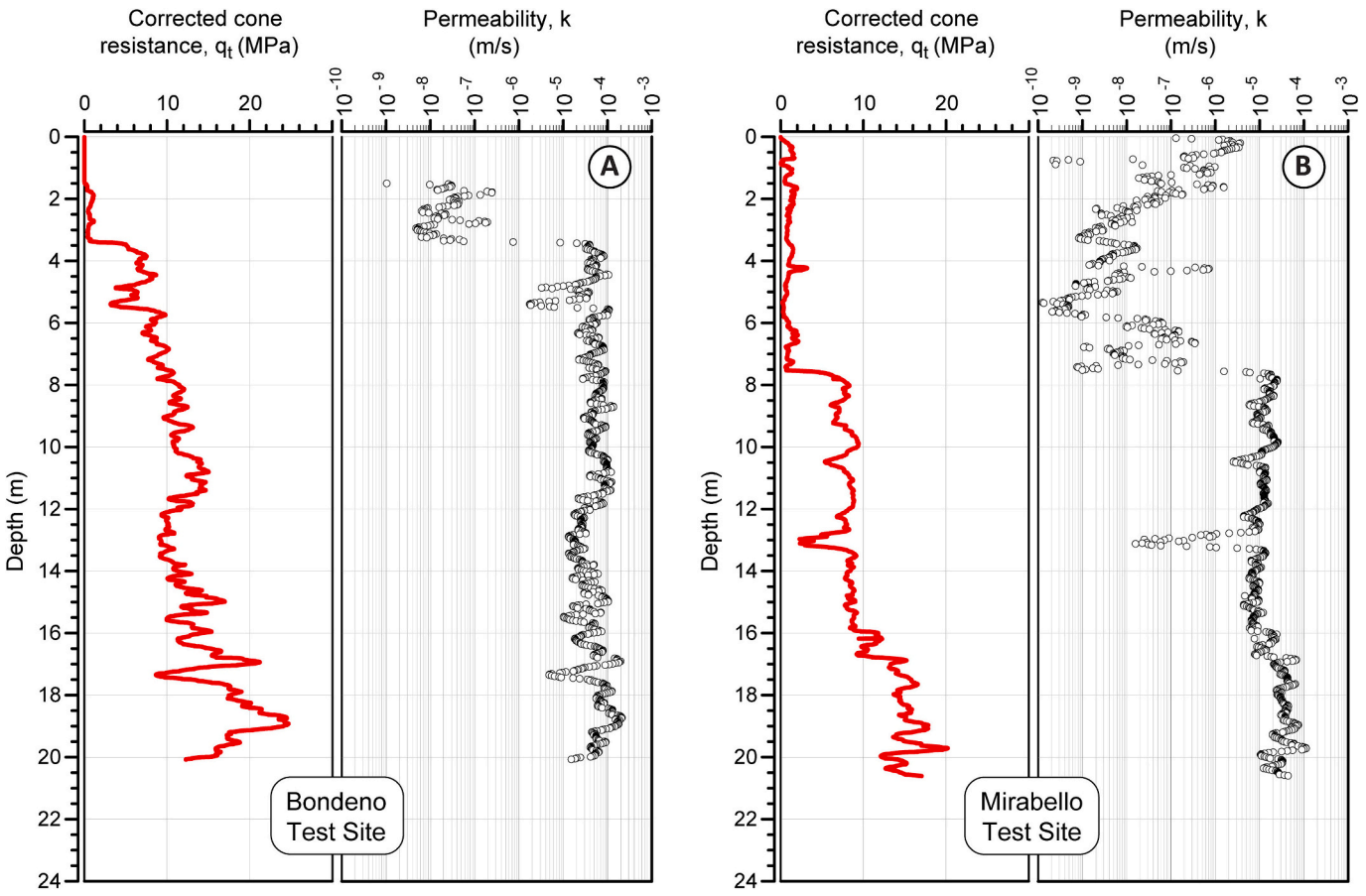

Fig. 6. CPTU-based predicted values of permeability for (a) the Bondeno blast test site subsoil and (b) the Mirabello blast test site subsoil.

Fig. 7. Cut sections of sand volcanoes induced by blast showing the internal features with a multiple gradation types and fine-grained veneer. Samples SB PPT5 (a), (b) and SB BH11 (c).

2019).

In the peripheral area of the natural panel and in the improved panel, the ejection products consisted only in small, thin, irregular, discontinuous, sand sheets.

4.3. Grain size analysis

As shown in Fig. 8a, the S01 core samples show a wide grain-size range, from medium to very fine sands and silty sands. From bottom to top, the sediment sequence generally starts with silty sand (14.8 m), overlain by coarser medium sands (12.9–13.5 m). A thin layer of very fine sandy silt is present at 11.7 m depth, overlain by medium to fine sand (11.2–5.4 m), which is in turn covered by sandy silt in the topmost part of the profile. Core S11 (Fig. 8a) is characterized by homogeneous grain size in the range of medium sands. Core S501 shows the finest sediments ranging from sandy silts to silty sands. Compared to Mirabello (Fontana et al., 2019) the Bondeno samples show an overall coarser grain-size.

As visible in Fig. 8b, the sand blows show a narrower range of grain-size distribution and are typically medium sand except for sample SBBH12 from a peripheral smaller volcano, which is finer grained and less sorted. In the two cases where the deposits have been sub-sampled vertically, the grain-size curves show a slightly more fine-grained fraction moving from the bottom to the top. A narrowing of the grain-size range of the sand blows, impoverished in the finer grained portion with respect to the source layers, was observed also in Mirabello.

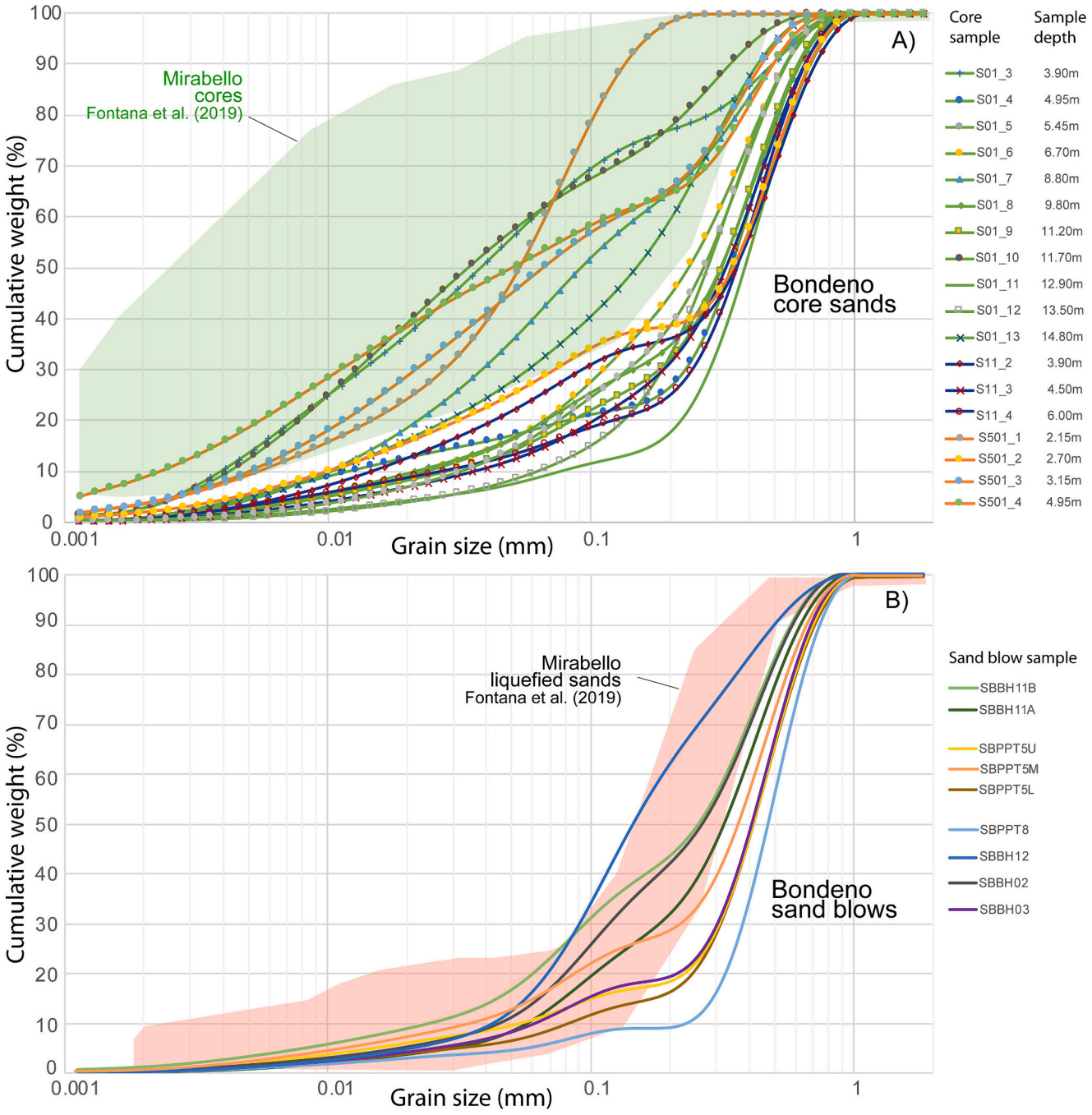

Fig. 8. Grain-size distribution curves of samples collected from the boreholes (a) and from the sand ejecta (b) in the Bondeno area. The grain-size colored spectra of Mirabello cores (a) and sand blows (b) is also shown.

Table 1
Soil index properties based on grain size distribution curves.

Description	Sample	Depth (m)	FC (%)	D_{60} (mm)	D_{30} (mm)	D_{10} (mm)	U	C	USCS
Borehole S01	S01_3	3.90	64.44	0.06	0.01	0.00	15.31	0.77	CL
Borehole S01	S01_4	4.95	19.30	0.22	0.23	0.01	17.11	18.87	SM
Borehole S01	S01_5	5.45	19.81	0.33	0.14	0.03	9.71	1.81	SM
Borehole S01	S01_6	6.70	21.99	0.30	0.11	0.02	11.99	1.72	SM
Borehole S01	S01_7	8.80	45.43	0.15	0.04	0.01	14.68	0.96	SM
Borehole S01	S01_8	9.80	21.36	0.37	0.15	0.02	16.32	2.61	SM
Borehole S01	S01_9	11.20	18.32	0.37	0.18	0.03	12.27	3.02	SM
Borehole S01	S01_10	11.70	63.77	0.06	0.01	0.00	13.80	0.66	CL
Borehole S01	S01_11	12.90	9.60	0.44	0.28	0.08	5.39	2.25	SM-SP
Borehole S01	S01_12	13.50	11.49	0.33	0.19	0.07	5.01	1.66	SM-SP
Borehole S01	S01_13	14.80	34.72	0.20	0.06	0.01	18.96	1.57	SM
Borehole S11	S11_2	3.90	27.11	0.43	0.09	0.02	27.95	1.36	SM
Borehole S11	S11_3	4.50	15.83	0.39	0.19	0.04	10.16	2.46	SM
Borehole S11	S11_4	6.00	16.08	0.41	0.24	0.03	14.23	4.95	SM
Borehole S501	S501_1	2.15	66.60	0.07	0.03	0.01	12.31	2.09	CL
Borehole S501	S501_2	2.70	30.74	0.41	0.07	0.01	42.08	1.28	SM
Borehole S501	S501_3	3.15	52.88	0.12	0.02	0.00	25.14	0.73	CL
Borehole S501	S501_4	4.95	55.27	0.12	0.01	0.00	50.91	0.46	CL
Sand boil SBBH11, upper portion (blast natural panel)	SBBH11A	–	14.06	0.38	0.19	0.05	7.37	1.73	SM
Sand boil SBBH11, lower portion (blast natural panel)	SBBH11B	–	24.53	0.33	0.10	0.03	12.88	1.11	SM
Sand boil SBBH12 (blast natural panel)	SBBH12	–	22.93	0.19	0.09	0.04	4.39	1.02	SM
Sand boil PPT4 (blast natural panel)	SBPPT4	–	28.34	0.41	0.10	0.01	48.52	2.96	SM
Sand boil PPT5, lower portion (blast natural panel)	SBPPT5L	–	9.03	0.47	0.31	0.09	5.54	2.46	SM-SP
Sand boil PPT5, medium portion (blast natural panel)	SBPPT5M	–	17.62	0.43	0.22	0.04	11.87	3.21	SM
Sand boil PPT5, upper portion (blast natural panel)	SBPPT5U	–	12.26	0.42	0.31	0.06	7.42	4.09	SM
Sand boil PPT8 (blast natural panel)	SBPPT8	–	6.13	0.52	0.38	0.24	2.22	1.17	SM-SP
Sand boil SBBH02 (blast improved panel)	SBBH02	–	18.42	0.34	0.12	0.05	7.31	0.91	SM
Sand boil SBBH03 (blast improved panel)	SBBH03	–	12.00	0.46	0.31	0.06	7.35	3.18	SM

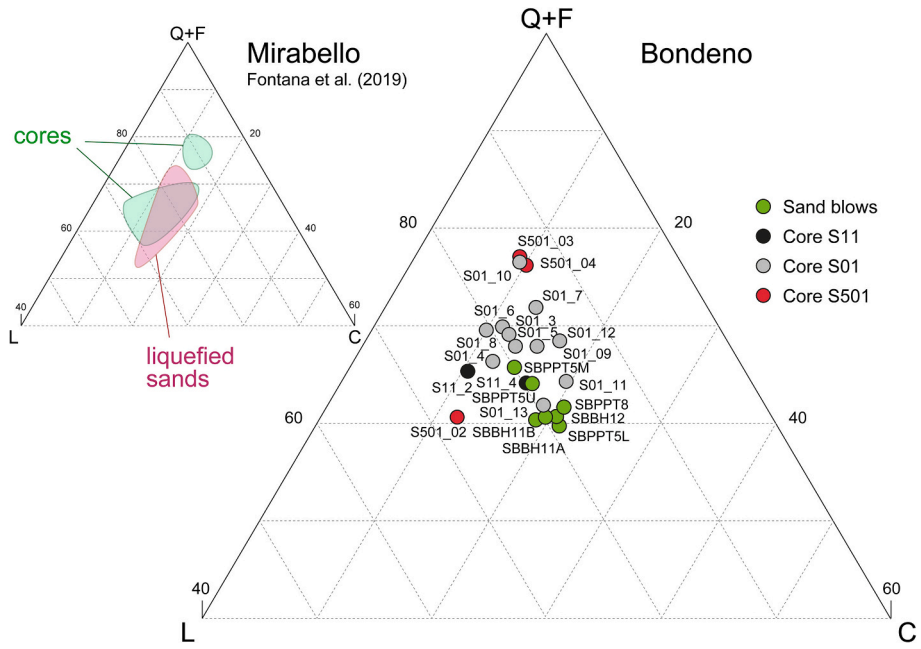

Fig. 9. Ternary diagrams showing the petrographic composition of the Bondeno core samples compared with Mirabello. Q: quartz; F: feldspars; L: siliciclastic rock fragments; C: carbonate rock fragments.

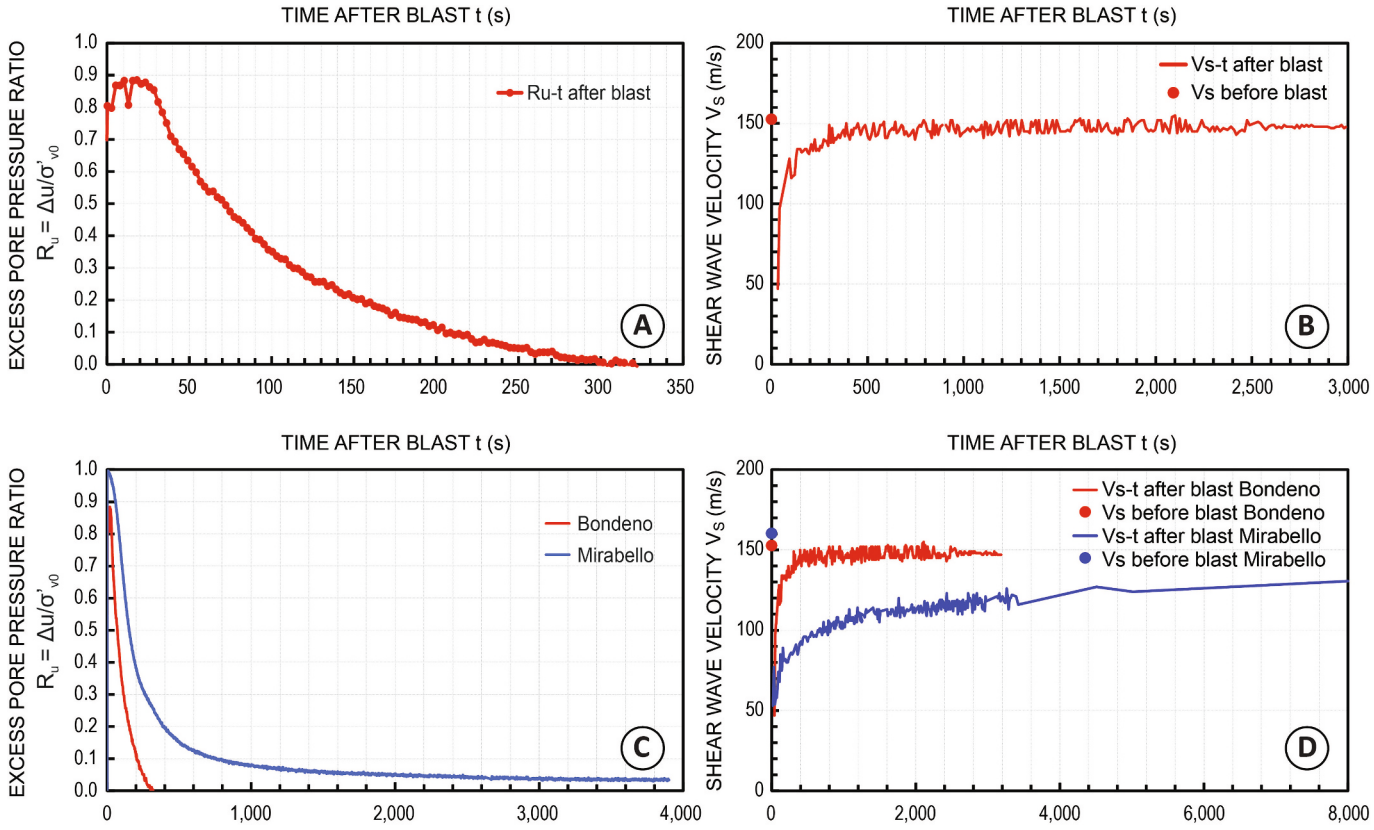

Fig. 10. R_u (PPT6, 5.84 m depth) (a) and V_s (SDMT blast, 6.10 m depth) (b) profiles vs time (Bondeno); comparisons between R_u (c) and V_s (d) vs. time (Bondeno PPT 5.84 m- SDMT blast 6.10 m & Mirabello PPT 7.5 m SDMT 7.25 m).

The index properties (FC, U, C), reported in Table 1 and used for the USCS classification, indicate that the non-liquefied crust are classified as silty clays (CL), while the liquefied sands from the boreholes, or collected as blasting ejecta, are most frequently classified as silty sand (SM), sometimes as poorly graded sand with silt (SP-SM), with FC between 10 and 45 %. Index U is typically below 15 and C varies between 1 and 3. The sand blows are generally cleaner (FC < 13 %) than the silty sand from cores (FC < 20 %).

4.4. Sand composition

The examined core sands are constantly quartz-feldspar-rich, Q + F is comprised from 50 to 70 % of whole sand grains, with higher values from 9 to 12 m depth and lower contents up-section (Fig. 9). Quartz consists mainly of single crystal and subordinate polycrystalline grains, feldspars are plagioclase and minor K-feldspar. Siliciclastic lithics (L) vary from 12 to 18 % and the shallowest sample of core S501 yields the maximum value of 23 %. Siliciclastic lithics are dominated by low grade metamorphic rocks (phyllites and micashist) associated with minor serpentinite, siltstones and shales. Spars of calcite represent the most common carbonate grains (C) associated with subordinate micrites. Carbonate lithics slightly increase in the deepest samples (from 13 to 15 m), where they make up 15 to 17 % of the whole sand sample. Lower values are observed in the sand up-section (2.5 to 5 m). Other components include micas (muscovite, biotite and chlorite) and heavy minerals (largely garnet), whose abundance is highly variable (up to 24 %).

Samples from sand boils show a quite homogeneous composition roughly matching that of sands from the deepest part of the cores (13 to 15 m).

By comparing the composition of the examined core sands with modes of Holocene alluvial sands in the Po alluvial plain (Fontana et al., 2019; Bruno et al., 2021; Tentori et al., 2022; Minarelli et al., 2022) we observe an overall affinity with the Po River, as indicated by the relative abundance of quartz and feldspars and metamorphic detritus. The relatively higher percentage of carbonate lithics in the deepest samples (13–15 m) has been previously observed in the late Quaternary Po River sand bodies as described by Demurtas et al. (2022) in the central sector of the Po plain.

In core S501 the quartz-feldspar-rich sands of the Po River paleochannel are overlain (S501_02) by slightly litharenitic sediments of Apennine affinity, possibly referable to the Secchia river.

4.5. Blast test shear wave velocity and pore pressure

During the blast, the excess pore pressure ratio R_u values were close to 1.0, indicating liquefaction in the natural panel from a depth of 4 to 9 m, as detailed by Rollins et al. (2021). In particular, Fig. 10a shows the R_u vs time curve computed from the PPT6 measurements acquired at 5.84 m depth. A R_u of about 0.9 persisted for 15 to 30 s, and then dissipated to near equilibrium values in about 4 min. Similarly, the shear wave velocity V_S, recorded in the natural panel during the blast, approximately at the same depth of PPT6, shows that V_S decreased to about 30 % of its pre-blast value ($V_S \approx 49$ m/s versus $V_S \approx 152$ m/s), recovering its initial value within a few minutes. Blast-induced liquefaction clearly reduces the vertical effective stress and alters the soil fabric, thus causing initial loss in soil stiffness (Mitchell and Solymar, 1984). However, the dissipation of the excess pore pressure allows the soil to reconsolidate into a denser and more stable configuration (Narin van Court and Mitchell, 1994) characterized by a higher soil stiffness, as

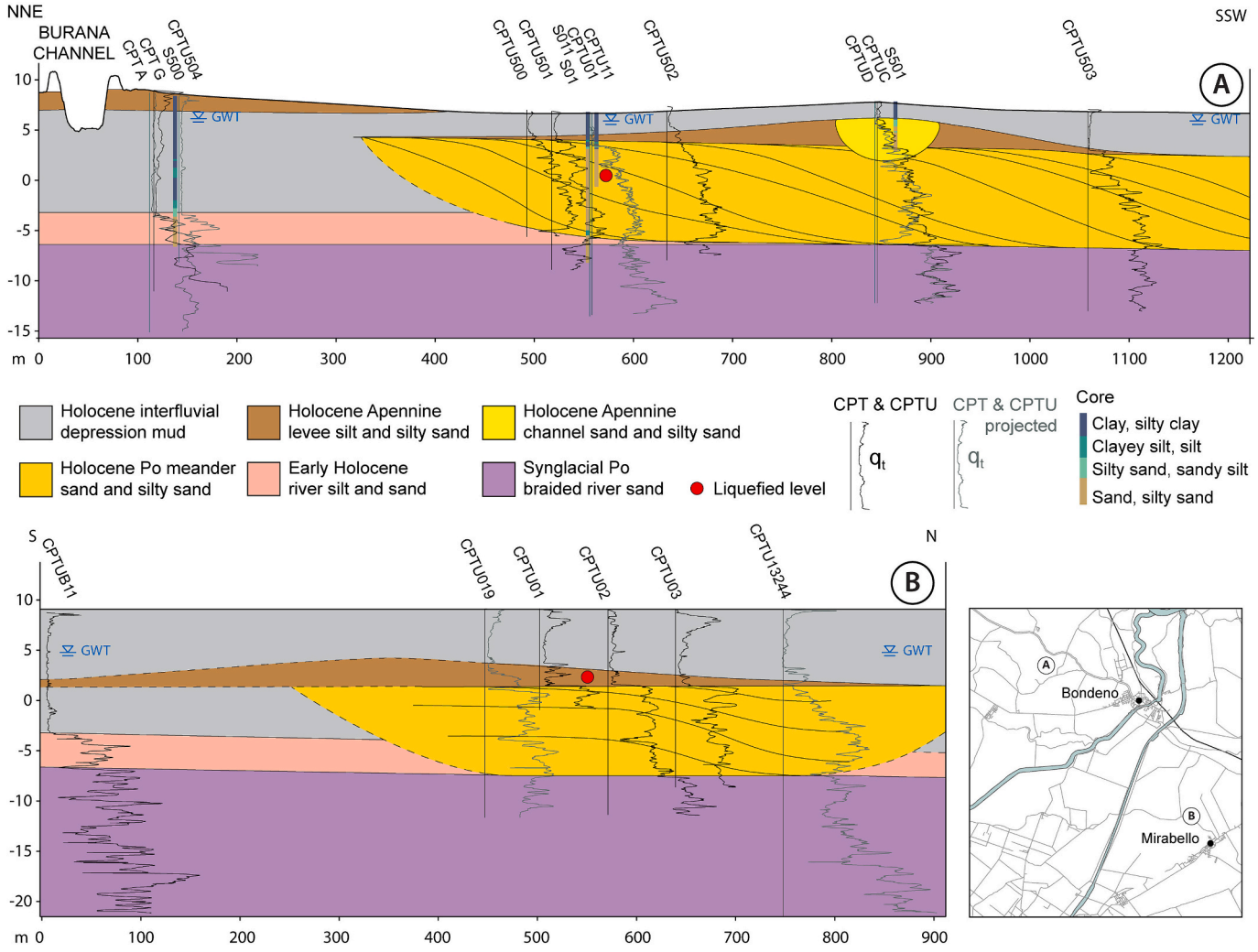

Fig. 11. Stratigraphic sections derived from the correlation of cores, CPT and CPTU logs at Bondeno (a), and Mirabello (b) test sites, showing the liquefaction source layers.

also confirmed at the Bondeno trial site by R_u and V_S data (Fig. 10a and b).

5. Discussions

The integrated interpretation of in situ tests (boreholes and CPTUs) and laboratory analyses performed in the Bondeno area has allowed an accurate reconstruction of the subsurface stratigraphic architecture to the depth of 20 m, with the identification of the different sedimentary bodies, their geometry, sediment grain-size, and composition. The correlation of these data has provided a 2D subsoil section extending approximately 1 km from NNE to SSW (Fig. 11a). The lower portion of the section is referable to the Po braided river sands from the Last Glacial Maximum, partially eroded and reworked by the Holocene meandering channel system. The main depositional body consists of a 10 m-thick sand channel-point bar unit, deposited by the Po River during the Holocene and extending laterally for at least 800 m. Sands vary from coarse to medium grained to silty sands and are quartz-rich in composition. The meander body is encased into flood plain mud deposits and pass upward to a thin and laterally-confined body of litharenitic fine-grained silty sand and sandy silt associated with levee and narrow channel facies of an Apennine tributary, the Secchia river. The sandy sediments are in turn covered by an argillaceous crust up to 3 m-thick deposited in a flood-plain environment.

A quite similar alluvial stratigraphic succession typifies the Mirabello study case (Fontana et al., 2019, Fig. 11b) made up of 9 m-thick sand channel-point bar system of the Po River (quartz-rich, medium to fine grained sands and silty sands) covering the last glacial fluvial sands. These deposits are replaced upward by thin (2 m) and laterally confined bodies of fine-grained silty sand and sandy silt, referable to levee and narrow channel facies of the Reno River. In the Mirabello case, the sandy sediments are covered by a thicker, up to 6 m, argillaceous crust of flood-plain depositional environment.

With respect to the source horizon identification, at Bondeno the liquefaction was induced in medium-coarse sands and silty sands of the Po River channel and point-bar, below 3 m in depth. As mentioned in section 4.1, the permeability of this soil unit was found to vary in a rather narrow interval between 10^{-5} and 10^{-4} m/s (with a mean value equal to $5.75{\cdot}10^{-5}$ m/s), with the exception of silty sand and silt intercalations, at times detected between 4 and 6 m, that are typically characterized by permeability values in the range $1.74{\cdot}10^{-6}$–10^{-5} m/s, i.e. one order of magnitude lower.

On the other hand, in the Mirabello case the ejected liquefied sediments involved the silty sand and sandy silt of the buried Reno River levee, from 6 to 8 m in depth. According to CPTU-based estimates, permeability characteristics of these sediments vary in a rather wide range (from approximately 10^{-9} to 10^{-5} m/s), likely as a consequence of the soil unit heterogeneity, with a computed mean value equal to $4{\cdot}10^{-6}$ m/s.

It is worth observing that in both experiments, the liquefaction phenomena generated an overall narrowing of the grain-size range of the sand blows with respect to the source layers.

Based on the measurements acquired at the Bondeno and Mirabello blast test sites, for similar depths and in natural soil conditions, further considerations can be carried out. The comparison between the R_u (Fig. 10c) and V_S (Fig. 10d) profiles highlights that the liquefaction process developed over a shorter time in Bondeno than in Mirabello. In Mirabello, the R_u dissipation took approximately 20 min and the V_S values got closer to its pre-blast value only about 21 h after the blast.

This different time of water dissipation is largely due to the presence and features of the argillaceous crust. In detail, at the Mirabello site, the crust is composed of two different cohesive layers. The upper four meters are strongly argillaceous and classified, according to USCS, as silty clay (CH) with fines content FC ≈ 100 % and plasticity index PI ≈ 31–58 %. The lower portion of the crust, between 4 and 6 m, consists of clayey silt with sand (CL to CH) with FC ≈ 70–80 % and PI = 23–27 % (Amoroso et al., 2017). Differently, at the Bondeno site, the crust is homogeneous and composed of a single layer, about 3 m-thick, classified as silty clay (CL), with lower fines content (FC ≈ 75–92 %), and lower plasticity (PI ≈ 18–22 %, Amoroso et al., 2022) compared to Mirabello. Moreover, the sand source layer in Bondeno has an overall coarser grain size, with FC ≈ 10–45 %, unlike the FC ≈ 25–75 % at the Mirabello site.

6. Final remarks

The research sites of Bondeno and Mirabello with a wide dataset from 2012 earthquake and full scale experiments allows the following considerations in the field of the engineering geology:

- The preeminent role in the liquefaction phenomena is played by subsoil sedimentary stacking pattern, in particular the lateral and vertical confinement of the sandy bodies, their thickness, and the presence, thickness and plasticity of an overlaying non-liquefiable crust;
- The petrographic composition of the sands allows us to discriminate the studied lithological units. Moreover, based on the compositional affinity, the petrography of the liquefied sands that ejected to the surface as sand boils, compared with that of buried sands, provides an important constraint in the recognition of the source layer. This is corroborated by the observation that the selective ejection mechanisms do not influence the sand composition, and that erosion or breakage of the most erodible grains due to the abrasive flow of sand grains are minor;
- The grain-size alone may not provide precise indications for the attribution of the source layer due to sorting effects occurring within dikes and later as the material is extruded. In fact, as observed both in blast-liquefied sands and in the 2012 earthquake sand boils, the segregation of the silt-clay fraction, following the generated excess pore water pressure, produced modifications in grain-size and generated better sorted sand;
- The delay in the excess pore water pressure dissipation recorded by the blast-induced liquefaction may be related to: (1) the thicker non-liquefied crust (≈ 6 m at Mirabello) compared to the thinner cohesive top-layer (≈ 3 m) in Bondeno; (2) the different soil plasticity of these silty-clayey caps; (3) the grain-size and therefore the permeability of the source layer; (4) the wider size of the permeable fluvial meander sand body in Bondeno, which more rapidly dissipated the liquefaction overpressure.

All these aspects may explain why the liquefaction phenomena, in Mirabello, where the source layer is thinner and laterally confined, lasted longer than in Bondeno, as observed during the blast test experiments. This suggests that liquefaction phenomena induced by the 2012 Emilia seismic sequence, scattered through the epicentral area, likely had variable durations in the different liquefaction sites according to the local stratigraphic architecture.

CRediT authorship contribution statement

Luca Minarelli: Writing – original draft, Supervision, Methodology, Investigation, Conceptualization. **Daniela Fontana:** Writing – original draft, Resources, Methodology, Formal analysis, Conceptualization. **Kyle M. Rollins:** Writing – review & editing, Resources, Investigation. **Marco Stefani:** Writing – original draft, Conceptualization. **Laura Tonni:** Writing – review & editing, Resources, Investigation. **Sara Amoroso:** Writing – original draft, Supervision, Project administration, Conceptualization.

Declaration of competing interest

The authors declare that they have no known competing financial interests or personal relationships that could have appeared to influence

the work reported in this paper.

Data availability

Some or all data, models, or code that support the findings of this study are available from the corresponding author upon reasonable request. The data include in situ and laboratory test results.

Acknowledgments

The study was primarily funded by Geopier Foundation Company (Davidson, North Carolina). A special thanks also to Releo s.r.l. (Ferrara, Italy), who provided the installation of the rammed aggregate piers. The in situ testing campaign was carried out by CIRI Edilizia e Costruzioni, University of Bologna, Italy, under the research project TIRISICO ("Tecnologie Innovative per la riduzione del rischio sismico delle Costruzioni", Project No. PG/2015/737636, POR-FESR 2014-2020). Financial contributions to this research activity were provided by INGV-FIRB Abruzzo project ("Indagini ad alta risoluzione per la stima della pericolosità e del rischio sismico nelle aree colpite dal terremoto del 6 aprile 2009"), by INGV-Abruzzo Region project ("Indagini di geologia, sismologia e geodesia per la mitigazione del rischio sismico", L.R. n. 37/2016), and by Alma Mater Studiorum—Università di Bologna within the AlmaIdea research project (2017, Coordination by Laura Tonni). Special thanks to Brigham Young University for contributing to the realization of the blast test experiment in terms of personnel and technical equipment; to Michele Perboni, who kindly guested the experimental activities; to the Bondeno Municipality and to the Emilia-Romagna Region, who provided all the necessary support to realize the research in collaboration with the other local authorities.

References

Amorosi, A., Bruno, L., Facciorusso, J., Piccin, A., Sammartino, I., 2016. Stratigraphic control on earthquake-induced liquefaction: a case study from the Central Po Plain (Italy). Sediment. Geol. 345, 42–53. https://doi.org/10.1016/j.sedgeo.2016.09.002.

Amoroso, S., Milana, G., Rollins, K.M., Comina, C., Minarelli, L., Manuel, M.R., Monaco, P., Franceschini, M., Anzidei, M., Lusvardi, C., Cantore, L., Carpena, A., Casadei, S., Cinti, F.R., Civico, R., Cox, B.R., De Martini, P.M., Di Giulio, G., Di Naccio, D., Di Stefano, G., Facciorusso, J., Famiani, D., Fiorelli, F., Fontana, D., Foti, S., Madiai, C., Marangoni, V., Marchetti, D., Marchetti, S.L., Martelli, L., Mariotti, M., Muscolino, E., Pancaldi, D., Pantosti, D., Passeri, F., Pesci, A., Romeo, G., Sapia, V., Smedile, A., Stefani, M., Tarabusi, G., Teza, G., Vassallo, M., Villani, F., 2017. The first Italian blast-induced liquefaction test (Mirabello, Emilia-Romagna, Italy): description of the experiment and preliminary results. Ann. Geophys. 60 (5). https://doi.org/10.4401/ag-7415.

Amoroso, S., Rollins, K.M., Andersen, P., Gottardi, G., Tonni, L., García Martínez, M.F., Wissmann, K., Minarelli, L., Comina, C., Fontana, D., De Martini, P.M., Monaco, P., Pesci, A., Sapia, V., Vassallo, M., Anzidei, M., Carpena, A., Cinti, F.R., Civico, R., Coco, I., Conforti, D., Doumaz, F., Giannattasio, F., Di Giulio, G., Foti, S., Loddo, F., Lugli, S., Manuel, M.R., Marchetti, D., Mariotti, M., Materni, V., Metcalfe, B., Milana, G., Pantosti, D., Pesci, A., Salocchi, A.C., Smedile, A., Stefani, M., Tarabusi, G., Teza, G., 2020. Blast-induced liquefaction in silty sands for full-scale testing of ground improvement methods: insights from a multidisciplinary study. Eng. Geol. 265. https://doi.org/10.1016/j.enggeo.2019.105437.

Amoroso, S., García Martínez, M.F., Monaco, P., Tonni, L., Gottardi, G., Rollins, K.M., Minarelli, L., Marchetti, D., Wissmann, K., 2022. Comparative study of CPTU and SDMT in liquefaction prone silty sands with ground improvement. J. Geotech. Geoenviron. Eng. 148 (6). https://doi.org/10.1061/(ASCE)GT.1943-5606.0002801.

Amoroso, S., Rollins, K.M., Minarelli, L., Monaco, P., Wissmann, K., 2024. Improved liquefaction resistance with rammed aggregate piers resulting from increased earth pressure coefficient and density. J. Geotech. Geoenviron. Eng. 150 (6). https://doi.org/10.1061/JGGEFK.GTENG-11727, 04024040.

ASTM D-2487-11, 2011. Standard Practice for Classification of Soils for Engineering Purposes (Unified Soil Classification System). American Society for Testing and Materials, USA.

ASTM D2488-09, 2009. Standard Practice for Description and Identification of Soils (Visual-Manual Procedure). American Society for Testing and Materials, USA.

Bertolini, I., Gottardi, G., Marchi, M., Tonni, L., Bassi, A., Rosso, A., 2022. Application of CPT to the evaluation of permeability in a Po river embankment prone to backward erosion piping. In: Proceedings 5th International Symposium on Cone Penetration Testing (CPT'22), Bologna, Italy, 8-10 June 2022, pp. 300–305. https://doi.org/10.1201/9781003308829-39.

Bol, E., Ozocak, A., Sert, S., Cetin, K.O., Arslan, E., Kocaman, K., Ayhan, B.U., 2024. Evaluation of soil liquefaction in the city of Hatay triggered after the February 6, 2023 Kahramanmaraş-Türkiye earthquake sequence. Eng. Geol. 229, 107648. https://doi.org/10.1016/j.enggeo.2024.107648.

Boulanger, R.W., Idriss, I.M., 2014. CPT and SPT based liquefaction triggering procedures. Report No. UCD/CGM-14/01. Department of Civil and Environmental Engineering, University of California, Davis, CA.

Bruno, L., Amorosi, A., Lugli, S., Sammartino, I., Fontana, D., 2021. Trunk river and tributary interactions recorded in the Pleistocene–Holocene stratigraphy of the Po Plain (northern Italy). Sedimentology 68 (6), 2918–2943. https://doi.org/10.1111/sed.12880.

Carminati, E., Martinelli, G., 2002. Subsidence rates in the Po Plain, northern Italy: the relative impact of natural and anthropogenic causation. Eng. Geol. 66 (3–4), 241–255.

Chang, W.J., Ni, S.H., Huang, A.B., Huang, Y.H., Yang, Y.Z., 2011. Geotechnical reconnaissance and liquefaction analyses of a liquefaction site with silty fine sand in Southern Taiwan. Eng. Geol. 123 (3), 235–245.

Civico, R., Brunori, C.A., De Martini, P.M., Pucci, S., Cinti, F.R., Pantosti, D., 2015. Liquefaction susceptibility assessment in fluvial plains using airborne LIDAR: the case of the 2012 Emilia earthquake sequence area (Italy). Nat. Hazards Earth Syst. Sci. 15, 2473–2483. https://doi.org/10.5194/nhess-15-2473-2015.

Demurtas, L., Bruno, L., Lugli, S., Fontana, D., 2022. Evolution of the Po–Alpine River system during the last 45 Ky inferred from stratigraphic and compositional evidence (Ostiglia, Northern Italy). Geosciences 12 (9). https://doi.org/10.3390/geosciences12090342.

Di Buccio, F., Comina, C., Fontana, D., Minarelli, L., Vagnon, F., Amoroso, S., 2023. Fines content determination through geotechnical and geophysical tests for liquefaction assessment in the Emilia alluvial plain (Ferrara, Italy). Soil Dyn. Earthq. Eng. 173. https://doi.org/10.1016/j.soildyn.2023.108057.

Emergeo Working Group, 2013. Liquefaction phenomena associated with the Emilia earthquake sequence of May–June 2012 (Northern Italy). Nat. Hazards Earth Syst. Sci. 13, 935–947. https://doi.org/10.5194/nhess-13-935-2013.

Fontana, D., Amoroso, S., Minarelli, L., Stefani, M., 2019. Sand liquefaction phenomena induced by a blast test: new insights from composition and texture of sands (late Quaternary, Emilia, Italy). J. Sediment. Res. 89 (1), 13–27. https://doi.org/10.2110/jsr.2019.1.

Giona Bucci, M., Villamor, P., Almond, P., Tuttle, M., Stringer, M., Ries, W., Smith, C., Hodge, M., Watson, M., 2018. Associations between sediment architecture and liquefaction susceptibility in fluvial settings: the 2010–2011 Canterbury Earthquake Sequence, New Zealand. Eng. Geol. 237, 181–197.

Güven, C., Wolf, L.W., Tuttle, M.P., Rogers, S.R., 2023. The influence of sedimentary architecture on the formation of earthquake-induced liquefaction features: a case study in the New Madrid seismic zone. Eng. Geol. 312, 106946. https://doi.org/10.1016/j.enggeo.2022.106946.

Hwanwoo, S., Han-Saem, K., Laurie, G.B., Byungmin, K., 2024. Geospatial liquefaction probability models based on sand boils occurred during the 2017 M5.5 Pohang, South Korea, earthquake. Eng. Geol. 329. https://doi.org/10.1016/j.enggeo.2024.107407.

Idriss, I.M., Boulanger, R.W., 2008. Soil Liquefaction during Earthquakes. MNO-12. Earthquake Engineering Research Institute, Oakland, CA.

Ishihara, K., 1985. Stability of natural deposits during earthquakes. In: Proceedings of 11th International Conference on Soil Mechanics and Foundation Engineering, San Francisco, pp. 321–376.

Kanibir, A., Ulusay, R., Aydan, O., 2006. Assessment of liquefaction and lateral spreading on the shore of Lake Sapanca during the Kocaeli (Turkey) earthquake. Eng. Geol. 83, 307–331.

Li, H., Liu, S., Tong, L., Xu, X., 2018. Investigating the resonant compaction effect on laterally loaded piles in layered soil. Eng. Geol. 246, 1–11.

Lugli, S., Marchetti Dori, S., Fontana, D., Panini, F., 2004. Composition of sands in cores along the high-speed rail (TAV): preliminary indications on the sedimentary evolution of the Modena plain. Alp. Mediterr. Quat. 17, 379–389.

Michetti, A.M., Giardina, F., Livio, F., Mueller, K., Serva, L., Sileo, G., Vittori, E., Devoti, R., Riguzzi, F., Carcano, C., Rogledi, S., Bonadeo, L., Brunamonte, F., Fioraso, G., 2012. Active compressional tectonics, Quaternary capable faults, and the seismic landscape of the Po Plain (northern Italy). Ann. Geophys. 55 (5), 969–1001. https://doi.org/10.4401/ag-5462.

Minarelli, L., Amoroso, S., Civico, R., De Martini, P.M., Lugli, S., Martelli, L., Molisso, F., Rollins, K.M., Salocchi, A., Stefani, M., Cultrera, G., Milana, G., Fontana, D., 2022. Liquefied sites of the 2012 Emilia earthquake: a comprehensive database of the geological and geotechnical features (Quaternary alluvial Po plain, Italy). Bull. Earthq. Eng. 20, 3659–3697. https://doi.org/10.1007/s10518-022-01338-7.

Mitchell, J.K., Solymar, Z.V., 1984. Time-dependent strength gain in freshly deposited or densified sand. J. Geotech. Eng. 110 (11), 1559–1576. https://doi.org/10.1061/(ASCE)0733-9410(1984)110:11(1559).

Narin van Court, W.A., Mitchell, J.K., 1994. Soil improvement by blasting. J. Explos. Eng. 12 (3), 34–41.

Obermeier, S.F., 1998. Liquefaction evidence for strong earthquakes of Holocene and latest Pleistocene ages in the states of Indiana and Illinois, USA. Eng. Geol. 50, 227–254. https://doi.org/10.1016/S0013-7952(98)00032-5.

Papathanassiou, G., Mantovani, A., Tarabusi, G., Rapti, D., Caputo, R., 2015. Assessment of liquefaction potential for two liquefaction prone areas considering the May 20, 2012 Emilia (Italy) earthquake. Eng. Geol. 189, 1–16.

Pesci, A., Teza, G., Loddo, F., Rollins, K.M., Andersen, P., Minarelli, L., Amoroso, S., 2022. Remote sensing of induced liquefaction: TLS and SfM for a full-scale blast test. ASCE J. Surv. Eng. 148 (1). https://doi.org/10.1061/(ASCE)SU.1943-5428.0000379, 04021026-1,23.

Pondrelli, S., Salimbeni, S., Perfetti, P., Danecek, P., 2012. Quick regional centroid moment tensor solutions for the Emilia 2012 (northern Italy) seismic sequence. Ann. Geophys. 55 (4), 615–621. https://doi.org/10.4401/ag-6146.

Quigley, M.C., Bastin, S., Bradley, B.A., 2013. Recurrent liquefaction in Christchurch, New Zealand, during the Canterbury earthquake sequence. Geology 41, 419–422. https://doi.org/10.1130/G33944.1.

Robertson, P.K., 2010. Estimating in-situ soil permeability from CPT & CPTu. In: Proc. 2nd Int. Symp. on Cone Penetration Testing, CPT'10, Huntington Beach, CA, 9-11 May 2010. https://www.geoengineer.org/storage/publication/18394/publication_file/2633/51Robehc.pdf.

Rollins, K.M., Amoroso, S., Andersen, P., Tonni, L., Wissmann, K.J., 2021. Liquefaction mitigation of silty sands using rammed aggregate piers based on blast-induced liquefaction testing. J. Geotech. Geoenviron. Eng. 147 (9), 04021085. https://doi.org/10.1061/(ASCE)GT.1943-5606.0002563.

Salocchi, A.C., Minarelli, L., Lugli, S., Amoroso, S., Rollins, K.M., Fontana, D., 2020. Liquefaction source layer for sand blows induced by the 2016 megathrust earthquake (Mw 7.8) in Ecuador (Boca de Briceno). J. S. Am. Earth Sci. 103. https://doi.org/10.1016/j.jsames.2020.102737, 102737-1,10.

Stefani, S., Minarelli, L., Fontana, A., Hajdas, I., 2018. Regional deformation of late Quaternary fluvial sediments in the Apennines foreland basin (Emilia, Italy). Int. J. Earth Sci. 107 (7), 2433–2447. https://doi.org/10.1007/s00531-018-1606-x.

Tentori, D., Mancini, M., Varone, C., Spacagna, R., Baris, A., Milli, S., Gaudiosi, I., Simionato, M., Stigliano, S., Modoni, G., Martelli, L., Moscatelli, M., 2022. The influence of alluvial stratigraphic architecture on liquefaction phenomena: a case study from the Terre del Reno subsoil (southern Po plain, Italy). Sediment. Geol. 440, 106258. https://doi.org/10.1016/j.sedgeo.2022.106258.

Tonni, L., Marchi, M., Bassi, A., Rosso, A., 2024. A sand boil database for piping risk management in the Po River, Italy. Water 16, 1384. https://doi.org/10.3390/w16101384.

Toscani, G., Burrato, P., Di Bucci, D., Seno, S., Valensise, G., 2009. Plio-Quaternary tectonic evolution of the Northern Apennines thrust fronts (Bologna-Ferrara section, Italy): Seismotectonic implications. Ital. J. Geosci. 128, 605–613. https://doi.org/10.3301/IJG. 2009.128.2.605.